Melting of mixtures in silica nanopores*

Joanna Czwartos[1], Malgorzata Sliwinska-Bartkowiak[1,‡],
Benoit Coasne[2], and Keith E. Gubbins[3]

[1]*Faculty of Physics, Adam Mickiewicz University, Poznan, Poland;*
[2]*Institut Charles Gerhardt Montpellier, CNRS and Université Montpellier 2,
Montpellier, France;* [3]*Center for High Performance Simulation and Department of
Chemical and Biomolecular Engineering, North Carolina State University,
Raleigh, NC 27695-7905, USA*

Abstract: We report experimental measurements of the melting of mixtures confined in nanoporous materials. Dielectric relaxation spectroscopy (DRS) was used to determine the solid–liquid phase diagram of bromobenzene/carbon tetrachloride (C_6H_5Br /CCl_4) mixtures confined in controlled pore glasses (CPGs) with an average pore diameter $H = 7.5$ nm. Our results show that the phase diagram of the confined mixture is of the same type as that for the bulk, but the solid–liquid coexistence lines are located at different temperatures. These results are compared with those previously obtained for CCl_4/C_6H_6 mixtures in activated carbon fibers (ACFs).

Keywords: confinement mixture; controlled pore glasses; freezing; melting; solid–liquid phase diagrams.

INTRODUCTION

Melting of pure fluids confined in nanoporous materials has been extensively studied using both experiments and simulations [1,2]. This effort is relevant to the fundamental understanding of the effect of confinement and surface forces on thermodynamics and dynamics of fluids. From a practical point of view, the freezing–melting of fluids in nanopores is relevant to applications that involve confined systems (lubrication, preparation of nanostructured materials, etc.). Of practical interest is the understanding of confinement effects on the lubricating properties of thin films in nanotechnologies (e.g., magnetic hard disks). Despite a few studies of molten salts [3,4] and colloidal mixtures [5], there seems to have been no study on the freezing of confined mixtures of simple fluids.

Recently, we studied the confinement effect on freezing–melting of mixtures confined in graphite nanopores, by means of Monte Carlo molecular simulations and experiments [6–8]. We found that the phase diagram for the confined mixture was of the same type as that for the bulk, but the solid–liquid coexistence lines were located at higher temperatures. This result was expected since previous experiments and simulations have shown that the freezing temperature of pure fluids confined in strongly attractive pores is larger than the bulk [9–11]. The aim of this work is to present the differences in melting behavior of mixtures confined in different kind of pores (e.g., silica mezopores).

The differences in melting point of liquids for silica and carbon mesopores can be discussed on the basis of our experimental and simulations results obtained for fluids of small molecules confined in pores [1,9,10]. The influence of energetics (fluid–fluid and fluid–wall interactions) on the melting behavior of the fluids confined in porous materials can be understood in terms of two main parameters, as proposed in our previous work [9]. One is the pore width H^*, which is expressed as a multiple of the diameter of the fluid molecule. The other is the parameter α, which is the ratio of the fluid–wall to the fluid–fluid attractive interaction, $\alpha = \dfrac{\rho_w \varepsilon_{fw} \sigma_{fw}^2 \Delta}{\varepsilon_{ff}}$, where Δ is the interlayer spacing in the solid and ρ_w is the number of the wall atoms per unit area. Thus, the value of α depends not only on the ratio of the two well depths, but also depends strongly on the density of wall atoms, the interlayer spacing, and the fluid-wall diameter parameter, σ_{fw}. The density is 114 nm^{-2} for carbon, but only half as much, 57 nm^{-2} for silica (density of surface oxygen atoms per unit area). In addition, Δ is considerably smaller for silica (0.22) than for carbon (0.33) [2,6]. While it is true that the fluid-wall energy well depth is larger for silica than for carbon, this effect is more than compensated for by the difference in surface density, $\sigma_{\phi\omega}$ and Δ, so that the values of α are usually higher for fluid-carbon than for fluid-silica. Our previous results [10], supported by other literature [11], indicate that the threshold α value for Lennard–Jones fluids in smooth-walled pores is 1.15; thus, for $\alpha \geq 1.15$ we expect (based on numerous simulation results for slit-shaped pores) an elevation in melting temperature, and a depression in melting temperature is expected for $\alpha \leq 1.15$. Thus, based on energetic considerations alone, we expect a decrease in a melting temperature of fluids of small molecules confined in silica pores and an increase in carbon pores. We note that the magnitude of the shift in melting temperature appears to be strongly dependent on the pore geometry.

In this paper, we report experiments for mixtures confined in silica pores. The solid–liquid phase diagram of the mixture was determined for both the bulk and the confined system in order to estimate the effect of confinement on the melting temperature and the solid–liquid phase diagram. The experimental measurements consist of dielectric relaxation spectroscopy (DRS) for bromobenzene/carbon tetrachloride (C_6H_5Br/CCl_4) confined in controlled pore glasses (CPGs) of an average pore diameter $H = 7.5$ nm, corresponding to a reduced pore size $H/\sigma \sim 15$ (σ is the size of the adsorbate molecule, $\sigma = 0.514$ nm for CCl_4).

EXPERIMENTAL TECHNIQUES

CPGs having a mean pore width of 7.5 nm were used in this work to study the melting upon confinement of C_6H_5Br/CCl_4 mixtures. Pores in this material, which are approximately of a cylindrical-shaped geometry, are expected to accommodate a dozen layers of CCl_4 or C_6H_5Br since the reduced pore width is $H^* \sim 15$ (using either the size of CCl_4 or C_6H_5Br). CCl_4 and C_6H_5Br were distilled twice prior to their use in experiments. Samples were outgassed during 5 days at a temperature of 150 °C and under a vacuum of 10^{-4} Torr, prior to introduction of the mixture. DRS of the confined mixture was performed using a parallel plate capacitor of empty capacitance $C_0 = 69.1$ pF. The capacitance C and the tangent loss tan(δ) (where δ is the angle by which current leads the voltage) of the filled sample were measured at different temperatures using a Solartron 1260 impedance–gain phase analyzer in the frequency range 10 Hz – 10 MHz. The real and imaginary parts of the complex dielectric permittivity $\varepsilon^* = \varepsilon' - i\varepsilon''$ are related to the capacitance and tangent loss of the system, $\varepsilon' = C/C_0$ and $\varepsilon'' = \tan(\delta)/\varepsilon'$ [12–15]. Melting of a solid phase can be monitored in the DRS experiment by a large increase of the permittivity. The sample was introduced between the capacitor plates as a suspension of CPG filled with the mixture in the bulk mixture. Therefore, the measurements yield an effective permittivity that has contributions from the bulk and the confined mixtures. During the experiments, the temperature of the sample was controlled with an accuracy of 0.1 K using a cryostat MK-70. A Perkin-Elmer DSC7 (differential scanning calorimeter) was used to determine the melting temperatures, by measuring the heat release in the

melting of confined C_6H_5Br/CCl_4 mixtures. The temperature scale of the DSC was calibrated to the melting temperatures of pure CCl_4 and C_6H_5Br, respectively. The melting temperatures were determined from the positions of the peaks of the heat flow signal. The melting temperatures were reproducible to within 0.5 K

RESULTS

Melting of C_6H_5Br/CCl_4 bulk mixtures or confined in CPG was determined by monitoring changes in the dielectric permittivity ε that occur at the transition from the solid to the liquid phases. Freezing of dipolar liquids such as bromobenzene is accompanied by a rapid decrease in ε' (the real part of the dielectric permittivity). Below the freezing point, the rotational phase ceases to exist, and ε' is almost equal to n^2 (n is the refractive index) as it is only related to deformation polarization. On the other hand, the maximum value ε'_m of the permittivity is obtained for the liquid phase. As a result, ε'_m and ε'_s (the real part of the permittivity in the solid phase) can be determined by measuring the functions $\varepsilon'(T)$ or $C(T)$ (C is the electric capacity of the system) in the vicinity of the melting point of a dipolar liquid. In turn, the determination of the temperature at which changes are observed in $\varepsilon(T)$ or $C(T)$ allows us to estimate the phase diagram of the system $(T,x_2)_p$. The electric capacity C of bromobenzene mixture with carbon tetrachloride was measured in the whole concentration range and over a wide range of temperatures. The mixtures were first cooled down to solid state and then transformed into the liquid phase by gradually increasing the temperature. The capacity C of the system was measured during the entire process. Figure 1 shows the curve $C(T)$ obtained for C_6H_5Br/CCl_4 bulk mixtures of various molar compositions. The melting process from the solid state (characterized by the minimum value of C, which is almost temperature-independent) to the liquid state occurs over a wide temperature range. This temperature range becomes narrower with increasing x_2 (x_2 is the mole fraction of bromobenzene). A sharp decrease in $C(T)$ is observed for $x_2 \sim 0.48$. On the other hand, a temperature broadening of the phase transition is observed for $x_2 \sim 0.48$. Assuming that T_2 [i.e., the temperature of the change in the monotonic character of $C(T)$] corresponds to the beginning of the melting process and taking T_1 as the temperature at which the transition into the homogeneous liquid state is complete, we obtain the phase diagram (T,x_2) of the mixture.
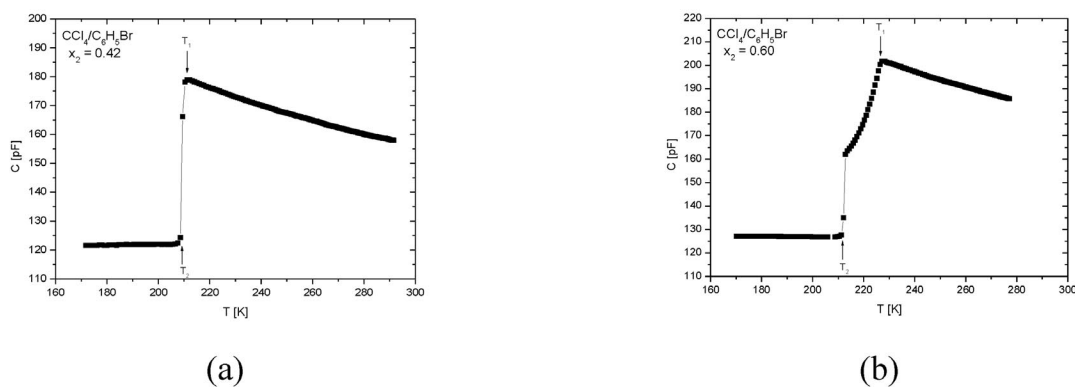

Fig. 1 Capacity curve $C(T)$ as a function of temperature for bulk C_6H_5Br/CCl_4 mixtures of various compositions (x_2 is the bromobenzene mole fraction): (a) $x_2 = 0.42$ and (b) $x_2 = 0.60$. T_2 corresponds to the beginning of the melting process while T_1 is the temperature at which the transition into the homogeneous liquid state is complete.

Figure 2 shows the phase diagram of the bulk C_6H_5Br/CCl_4 mixture. Such a phase diagram is characteristic of a simple eutectic mixture. The lines AEB were obtained from the temperature T_1 as it corresponds to the temperature at which the entire system is in the liquid state. The lines AE and BE correspond to the temperatures at which the liquid mixture is in equilibrium with a solid phase. The line CD was obtained from the temperature T_2 at which the system starts melting. The eutectic E indicates the point where the solid constituent rich in C_6H_5Br and that rich in CCl_4 are in equilibrium with the liquid phase having a composition $x_2^E \sim 0.48$. In the case of C_6H_5Br/CCl_4 mixtures, the melting points of the two components are rather close (bromobenzene, 242.3 K, and carbon tetrachloride, 252.4 K) so that the eutectic concentration x_2^E is very close to 0.5, which suggests that the properties of the system are close to those of the model of ideal miscibility.
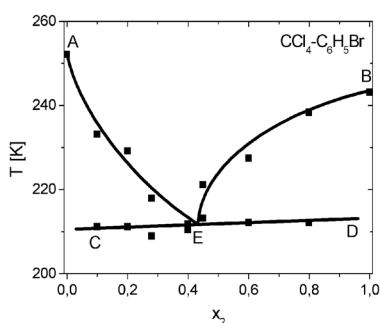

Fig. 2 Solid–liquid phase diagram (T,x_2) at constant pressure $P = 1$ atm for bulk C_6H_5Br/CCl_4 mixtures. (x_2 is the bromobenzene mole fraction). The lines between the symbols are provided as a guide for the eye.

The melting of C_6H_5Br/CCl_4 mixtures confined in CPG was also studied by monitoring the capacity curve $C(T)$ as a function of the temperature (Fig. 3). The sample is introduced as a suspension of porous glass particles in bulk mixtures so that the signal is both for the bulk and confined system. Starting from the solid phase, C exhibits two sudden changes as the temperature increases. For pure bromobenzene (Fig. 3c), the sharp increase at 229.8 K is attributed to the melting in pores, while that at 243.1 K corresponds to the melting of bulk bromobenzene. For the C_6H_5Br/CCl_4 mixtures confined
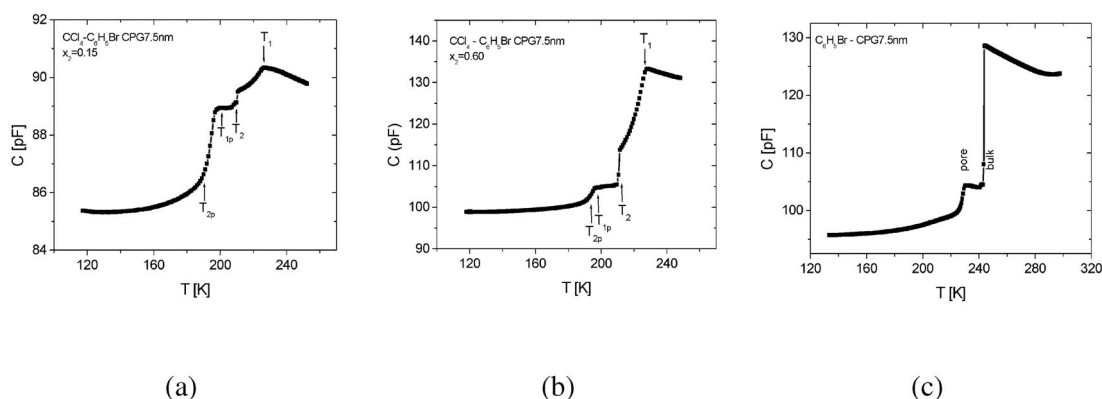

(a)   (b)   (c)

Fig. 3 Capacity curve $C(T)$ as a function of temperature for C_6H_5Br/CCl_4 mixtures confined in CPGs of various compositions (x_2 is the bromobenzene mole fraction): (a) $x_2 = 0.15$ and (b) $x_2 = 0.60$; (c) capacity curve $C(T)$ as a function of temperature for pure C_6H_5Br confined in CPG . The sample is introduced as a suspension of porous glass particles in the bulk mixture so that the signal is both for the bulk and the confined system.

in CPG (Figs. 3a and 3b), T_1 corresponds to the temperature at which melting is complete, while T_2 is the temperature at which the solid phase starts melting. The changes observed in the capacity curves at low temperatures T_{1P} and T_{2P} are attributed to the melting in pores.

In order to confirm the melting temperatures estimated from our dielectric relaxation measurements, we performed DSC measurements for C_6H_5Br/CCl_4 mixtures confined in CPG. The results were found to be independent of the heating rate in the range 0.5–10 K/min. The DSC scans for melting of C_6H_5Br/CCl_4 in CPG are shown in Figs. 4a–c. Four DSC endothermic peaks are observed, which are related with the following transition temperatures T_1, T_2, T_{1p}, and T_{2p}, obtained also from DRS method. The signals corresponding to the melting of the bulk mixture correspond to temperatures T_1 and T_2. The two additional peaks at T_{1p} and T_{2p} correspond to the liquidus and solidus lines for the mixture confined in CPG. For the bulk concentration $x_2 = 0.70$, only one peak is observed for the melting of the confined mixture, i.e., $T_{1p} \sim T_{2p}$. Such a behavior indicates that the molar composition of the mixture in the pores corresponds to the eutectic concentration x_{2p}^E. The temperatures of solidus–liquidus points obtained using the DSC method were consistent with those obtained from the DRS method.
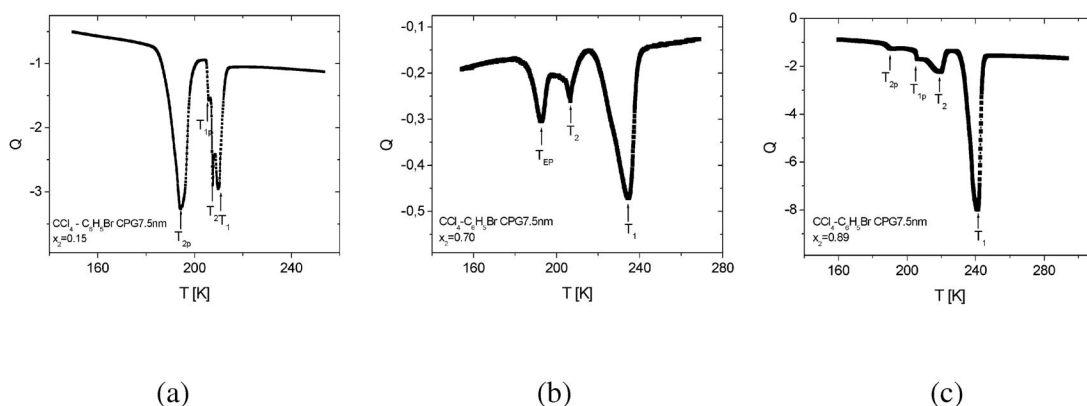

Fig. 4 (a–c) DSC scans of the melting of C_6H_5Br/CCl_4 mixtures confined in CPG for various concentrations : (a) $x_2 = 0.15$, (b) $x_2 = 0.70$, and (c) $x_2 = 0.89$. The sample is introduced as a suspension of porous glass particles in the bulk mixture so that the signal is both for the bulk and the confined system.

The phase diagram for the C_6H_5Br/CCl_4 mixture confined in CPG is compared with its bulk (Fig. 2) counterpart in Fig. 5. Similarly as the diagram presented in Fig. 2, the phase diagram for the C_6H_5Br/CCl_4 mixture confined in CPG is constructed on the basis of DRS results, confirmed also by DSC experiments. Our experimental results show that the phase diagram of the confined mixture is of the same type as that for the bulk (eutectic mixture). The melting temperature of CCl_4 confined in CPG is 236.2 K, while that of C_6H_5Br confined in CPG is 229.8 K. These in pore melting temperatures suggest that the eutectic concentration x_{2p}^E in pores is shifted toward the component having the lower melting point, i.e., C_6H_5Br. Our results suggest that $x_{2p}^E \sim 0.70$, which is larger than the bulk eutectic $x_2^E \sim 0.48$. We also observe that the melting temperature of the confined mixtures is lower than the bulk (the eutectic temperatures are 193.8 and 214.3 K for the confined and bulk mixtures, respectively). This behavior is typical of systems for which the ratio of the wall–fluid to the fluid–fluid interactions is lower than 1.
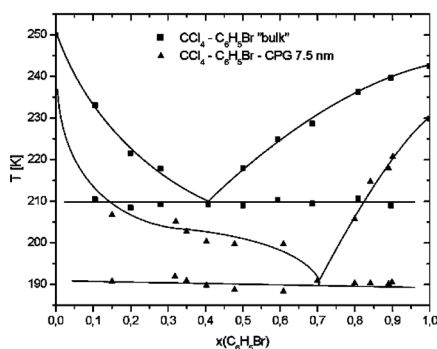
Fig. 5 Solid–liquid phase diagrams (T,x_2) at constant pressure $P = 1$ atm for C_6H_5Br/CCl_4 mixtures. x_2 is the bromobenzene mole fraction. The squares are for the bulk mixture (Fig. 2), while the triangles are for the mixture confined in CPG. The lines between the symbols are provided as a guide for the eye.

CONCLUSION

In this work, we report experiments on melting of mixtures confined in silica nanopores. Both dielectric and calorimetric experiments were used to determine the solid–liquid phase diagram of CCl_4/C_6H_5Br mixtures confined in CPG (silica) with an average pore diameter $H = 7.5$ nm ($\sim 15\sigma_{CCl4}$). We show that the phase diagram of the confined mixture is of the same type as that for the bulk. For the experimental system considered in this study, we found that the melting temperatures for the confined mixtures are lower than those for the bulk. This result was expected on the basis of the value of α parameter for fluids confined in silica pores, which is smaller than for liquids confined in graphite pores [9,16,17]. These results are consistent with those obtained for the azeotrope mixture (CCl_4/C_6H_6) confined in activated carbon fibers (ACFs) with an average pore diameter $H = 1.4$ nm, where an elevation of melting temperature of mixture relatively to the bulk was observed [17]. For both systems studied (e.g., the eutectic mixture in CPG and the azeotrope mixture in ACFs), we found that the phase diagrams of the confined mixture are of the same type as that for the bulk. On the other hand, for both systems studied it was also observed that azeotropic concentration (for mixture in ACF) as well as the eutectic concentration presented in this work are shifted relative to the bulk, toward the component with lower fluid–wall interactions. We can conclude that the shift of melting temperatures of liquid mixtures confined in slit carbon pores (ACFs) and cylindrical silica pores (CPGs) observed experimentally, can be understood in terms of the energetic α parameter, as it was shown for the confined fluids [18].

We are currently performing molecular simulations of eutectic mixtures confined in silica nanopores, in order to compare our simulation data with the experiments reported in the present work. Although the use of the parallel tempering technique greatly reduces the risk of being trapped in a metastable state, we plan to combine the present simulations with free energy calculations to corroborate our findings. Further experiments are also needed to clarify the nature of the confined phases. X-ray diffraction or neutron scattering will allow us to determine the structure of the confined phases.

ACKNOWLEDGMENTS

REFERENCES

1. L. D. Gelb, K. E. Gubbins, R. Radhakrishnan, M. Sliwinska-Bartkowiak. *Rep. Prog. Phys*. **62**, 1573 (1999).
2. C. Alba-Simionesco, B. Coasne, G. Dosseh, G. Dudziak, K. E. Gubbins, R. Radhakrishnan, M. Sliwinska-Bartkowiak. *J. Phys. Condens. Matter* **18**, R15 (2006).
3. R. R. Meyer, J. Sloan, R. E. Dunin-Borkowski, A. I. Kirkland, M. C. Novotny, S. R. Bailey, J. L. Hutchinson, M. L. H. Greene. *Science* **289**, 1324 (2000).
4. M. Wilson. *J. Chem. Phys*. **116**, 3027 (2002).
5. S. T. Cui, C. McCabe, P. T. Cummings, H. D. J. Cochran. *J. Chem. Phys*. **118**, 8941 (2003).
6. B. Coasne, J. Czwartos, K. E. Gubbins, F. R. Hung, M. Sliwinska-Bartkowiak. *Mol. Phys*. **102**, 2149 (2004).
7. B. Coasne, J. Czwartos, K. E. Gubbins, F. R. Hung, M. Sliwinska-Bartkowiak. *Adsorption* **11**, 301 (2005).
8. K. E. Gubbins, B. Coasne, J. Czwartos, M. Sliwinska-Bartkowiak. *J. Phys. Chem. C* (2009). In press.
9. R. Radhakrishnan, K. E. Gubbins, M. Sliwinska-Bartkowiak. *J. Chem. Phys*. **112**, 11048 (2000).
10. R. Radhakrishnan, K. E. Gubbins, M. Sliwinska-Bartkowiak. *J. Chem. Phys*. **116**, 1147 (2002).
11. R. Radhakrishnan, K. E. Gubbins, M. Sliwinska-Bartkowiak. *Phys. Rev. Lett*. **89**, 07610 (2002).
12. A. Chelkowski. *Dielectric Physics*, Elsevier, North-Holland, New York (1980).
13. M. Sliwinska-Bartkowiak, J. Gras, R. Sikorski, R. Radhakrishnan, L. Gelb, K. E. Gubbins. *Langmuir* **15**, 6060 (1999).
14. M. Sliwinska-Bartkowiak, G. Dudziak, R. Sikorski, R. Gras, R. Radhakrishnan, K. E. Gubbins. *J. Chem. Phys*. **114**, 250 (2001).
16. R. Radhakrishnan, K. E. Gubbins, A. Watanabe, K. Kaneko. *J. Chem. Phys*. **111**, 9058 (1999).
17. J. Czwartos, B. Coasne, K. E. Gubbins, F. R. Hung, M. Sliwinska-Bartkowiak. *Mol. Phys*. **103**, 3103 (2005).
18. M. Sliwinska-Bartkowiak, M. Jazdzewska, K. E. Gubbins, L. Huang. *Phys. Chem. Chem. Phys*. **10**, 4909 (2008).